ACCSCIENCE PUBLISHING

International Journal of Bioprinting

ACCEPTED PAPER · MAIN TEXT

Construction of a 3D-printed polycaprolactone scaffold functionalized with extracellular matrix and an MSC-affinity peptide for articular cartilage repair

Article ID: IJB026250258

Citation: Zhao X, Liu X, Huang Z, Ding K, Zhao Y, Bi Z. Construction of a 3D-printed polycaprolactone scaffold functionalized with extracellular matrix and an MSC-affinity peptide for articular cartilage repair. *Int J Bioprint.* 2026. doi: 10.36922/IJB026250258

AccScience Publishing
RESEARCH ARTICLE
Volume X Issue X (2026)
doi: 10.36922/IJB026250258

Construction of a 3D-printed polycaprolactone scaffold functionalized with extracellular matrix and an MSC-affinity peptide for articular cartilage repair

Running title: CM-MSC peptide functionalized 3D PCL scaffold

Xinqiang Zhao[1], Xiaoning Liu[2], Zhen Huang[3], Kun Ding[1], Yantao Zhao[4]*, and Zhenggang Bi[1]*

[1] Department of Orthopaedic Surgery, The First Affiliated Hospital of Harbin Medical University, Harbin 150001, China

[2] Department of Nurtrition, Women and Children's Hospital of Qingdao University, Qingdao 266034, China

[3] Department of Joint surgery, Minda Hospital of Hubei Minzu University, Enshi 445000, China

[4] Senior Department of Orthopedics, The Fourth Medical Center of Chinese PLA General Hospital, Beijing 100048, China

***Corresponding authors:**
Zhenggang Bi (drbizhenggang@163.com)
Yantao Zhao (biodoctor1981@163.com)

Citation: Zhao X, Liu X, Huang Z, Ding K, Zhao Y, Bi Z. Construction of a 3D-printed polycaprolactone scaffold functionalized with extracellular matrix and an MSC-affinity peptide for articular cartilage repair. *Int J Bioprint.* 2026. doi: 10.36922/IJB026250258

Received: June 19, 2026
Revised: July 10, 2026
Accepted: July 13, 2026
Published online: July 13, 2026

Abstract

Cartilage damage has emerged as a major clinical challenge due to the limited intrinsic regenerative capacity of articular cartilage. Current cartilage repair strategies often rely on exogenous cells and growth factors to promote tissue regeneration; however, their clinical translation is hindered by high costs, complex manufacturing processes, and potential immunogenicity. Thus, the development of high-performance acellular tissue-engineering scaffolds has attracted increasing attention. In this study, we engineered a biomimetic ternary composite scaffold consisting of polycaprolactone (PCL), a bone marrow mesenchymal stem cell (BMSC)-affinity peptide, and cartilage extracellular matrix (ECM) to facilitate efficient cartilage regeneration through synergistic multifunctional effects. PCL scaffolds with well-defined porous architectures and favorable mechanical properties were fabricated using three-dimensional (3D) printing. Following surface functionalization with the mesenchymal stem cell (MSC)-affinity peptide E7, the scaffolds were further coated with decellularized cartilage ECM. This biomimetic design enhances cell adhesion, selectively recruits endogenous MSCs, and provides the structural support required for tissue regeneration. Moreover, the bioactive components and biochemical cues retained within the ECM promote chondrogenic differentiation. *In vitro* studies demonstrated that E7-modified PCL (E7-PCL) significantly enhanced MSC adhesion and recruitment. The ECM/E7-modified composite scaffold further promoted stem-cell adhesion, proliferation, chondrogenic differentiation, and extracellular matrix deposition while maintaining excellent biocompatibility and mechanical integrity. *In vivo*, implantation of the ECM/E7-PCL (E/E7-P) scaffold resulted in markedly improved cartilage repair compared with ECM/PCL (E/P) scaffolds and untreated controls. Overall, these findings from in vitro and rabbit in vivo experiments indicate that E/E7-P represents a promising acellular tissue-engineering candidate for cartilage defect regeneration, pending further validation in more comprehensive experimental models.

Keywords: Articular cartilage repair; BMSC affinity peptide; 3D printing; Peptide-modified polycaprolactone; Cartilage tissue engineering

1. Introduction

Articular cartilage defects are common orthopedic disorders that frequently progress to degenerative osteoarthritis, chronic joint pain, functional impairment, and progressive tissue deterioration [1-3]. However, effective cartilage regeneration remains a major challenge because articular cartilage is avascular, aneural, and possesses a limited intrinsic capacity for self-repair [4,5]. Current clinical treatments, including microfracture (MF), autologous chondrocyte implantation (ACI), matrix-assisted ACI (MACI), and osteochondral autograft transfer (OATS), provide varying degrees of symptomatic relief and tissue repair but remain limited by inconsistent long-term outcomes, high costs, and suboptimal patient satisfaction [6]. Hence, tissue-engineering approaches incorporating biomimetic scaffolds, bioactive molecules, and stem cell-based therapies have been extensively investigated as alternatives for cartilage regeneration [6].

Among these strategies, the recruitment of endogenous reparative cells has emerged as a particularly attractive approach for in situ cartilage regeneration [7]. The MF procedure, which stimulates the release of stem and progenitor cells from the bone marrow cavity, is widely used clinically to promote cartilage repair [7]. Nevertheless, the limited retention, migration, and survival of recruited cells at the defect site often result in unsatisfactory regenerative outcomes [8,9]. To overcome these limitations, bone marrow mesenchymal stem cell (BMSC)-affinity peptides have been developed as a promising means of enhancing endogenous stem-cell recruitment. These short functional peptides specifically recognize and bind to BMSCs, enabling their selective capture and retention at injury sites without the need for exogenous cell transplantation, complex cell manipulation, or ethical concerns. Through specific ligand-receptor interactions, BMSC-affinity peptides facilitate the in situ recruitment, immobilization, and functional regulation of endogenous stem cells, thereby maximizing the intrinsic regenerative potential of host tissues. Because cartilage defects encountered in clinical practice often exhibit irregular geometries, there is a growing demand for tissue-engineered scaffolds that can be customized to match defect morphology while achieving stable integration with the surrounding native cartilage [10,11].

Three-dimensional (3D) printing has emerged as a powerful fabrication technology in regenerative medicine, enabling the production of scaffolds with precisely controlled architectures, pore structures, and mechanical properties [12,13]. Polycaprolactone (PCL) is one of the most widely used materials for 3D-printed scaffolds owing to its excellent processability, favorable biocompatibility,

and suitable degradation profile. However, the hydrophobic surface and lack of bioactive cell-recognition motifs in pure PCL limit cell adhesion, proliferation, and chondrogenic differentiation, thereby restricting its effectiveness in cartilage repair [14]. To address these shortcomings, various surface-functionalization strategies have been explored. For example, the incorporation of cartilage-derived extracellular matrix (ECM) components into PCL scaffolds has been shown to significantly enhance BMSC chondrogenesis and cartilage-specific matrix formation [15,16]. In addition, stem cell-targeted recruitment strategies have gained increasing attention. Functional peptides such as RGD and YIGSR can improve cell-material interactions, while BMSC-specific affinity peptides, including E7 and P19 identified through phage-display screening, exhibit strong binding affinity toward BMSC surface receptors and effectively recruit endogenous stem cells to sites of injury [17,18]. These approaches eliminate the need for *ex vivo* cell expansion and transplantation, offering a minimally invasive strategy for cartilage regeneration.

Cartilage ECM, composed primarily of type II collagen, proteoglycans, and matrix-bound growth factors, provides a highly specialized microenvironment that supports chondrogenesis, matrix remodeling, and tissue integration. Hence, the incorporation of cartilage-derived ECM into tissue-engineering scaffolds has emerged as a promising biomimetic strategy for cartilage regeneration [19]. Unlike synthetic biomaterials, which often lack essential biological signals, native ECM closely replicates the biochemical and structural characteristics of the cartilage niche, thereby enhancing cell recruitment, chondrogenic differentiation, and functional matrix deposition. When processed using techniques such as decellularization and lyophilization, cartilage ECM can retain key bioactive components while maintaining favorable biocompatibility and mechanical properties. ECM-functionalized scaffolds have been shown to promote cartilage-specific matrix synthesis, reduce immunogenicity, and facilitate long-term tissue integration [20]. Furthermore, the intrinsic anti-angiogenic properties of cartilage ECM help preserve the avascular environment required for hyaline cartilage formation, thereby minimizing the risk of undesirable endochondral ossification.

Although previous studies have incorporated either ECM components or bioactive peptides into PCL scaffolds, most existing approaches provide only partial functionality and fail to achieve effective synergistic integration [21,22]. Current composite scaffold designs primarily focus on enhancing cell-material interactions while often overlooking the coordinated regulation of mechanical support, targeted stem-cell recruitment, and biochemical induction. For example, the

incorporation of ECM can improve the biological activity of PCL scaffolds but does not fully overcome the poor cell adhesion associated with the hydrophobic PCL surface. Conversely, the grafting of nonspecific adhesion peptides, such as RGD, enhances cellular attachment but lacks selectivity for BMSCs, thereby limiting efficient endogenous stem-cell recruitment. Furthermore, many existing fabrication strategies rely on physical blending or simple surface coating, which may lead to heterogeneous distribution, rapid loss of bioactive components, and inadequate long-term stability. More importantly, the ability to actively direct endogenous BMSC homing, retention, and chondrogenic differentiation through rational biomaterial design remains a major challenge in cartilage tissue engineering [23]. Therefore, there is an urgent need to develop multifunctional scaffolds capable of integrating mechanical support, selective stem-cell recruitment, and biomimetic biochemical signaling within a single platform. [24].

To address these challenges, we developed a biomimetic ternary composite scaffold based on a novel "Mechanical Skeleton-Targeting Peptide-Natural Matrix" design concept. The scaffold consists of a 3D-printed PCL framework, a BMSC-affinity peptide, and cartilage-derived ECM. First, a porous PCL scaffold was fabricated using 3D printing to provide structural integrity and mechanical support. A previously validated BMSC-affinity peptide was then covalently immobilized onto the scaffold surface to facilitate the selective recruitment and retention of endogenous stem cells. Subsequently, decellularized cartilage-derived ECM was uniformly integrated into the scaffold through cross-linking, creating a biomimetic microenvironment enriched with native biochemical cues. We hypothesized that this multifunctional scaffold would promote cartilage regeneration through a synergistic mechanism involving sustained mechanical support, targeted BMSC recruitment, and ECM-mediated chondrogenic induction. Accordingly, the present study aimed to evaluate the ability of this composite scaffold to enhance articular cartilage repair, activate endogenous regenerative potential, and promote the formation and integration of hyaline cartilage-like tissue without the need for exogenous cell transplantation (**Figure 1**).

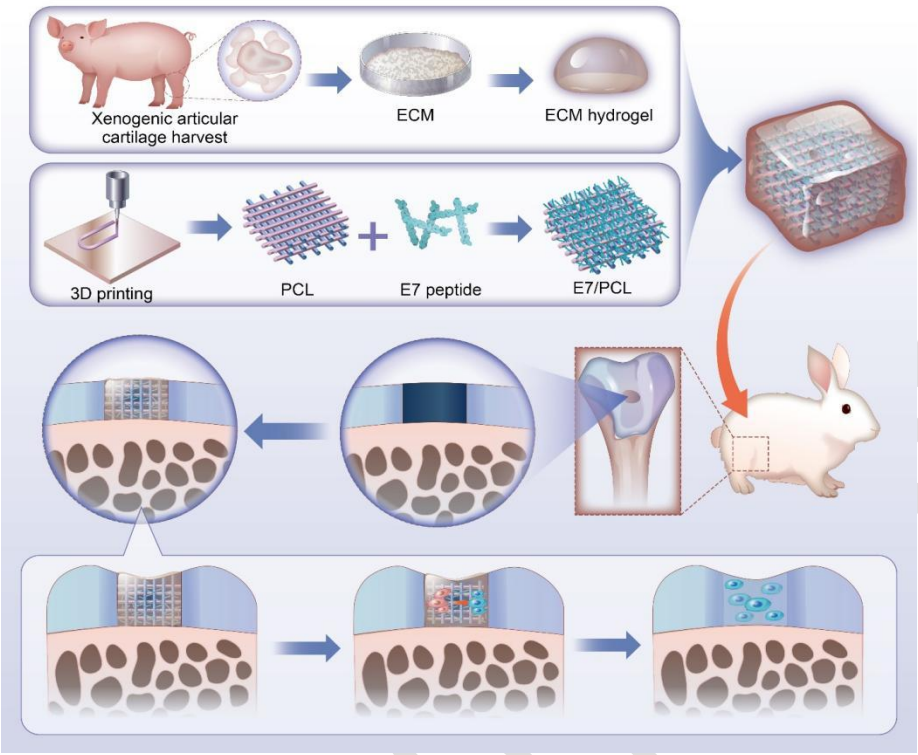

Figure 1. Schematic illustration of the 3D scaffold fabrication process and its application in cartilage tissue engineering.

2. Materials and methods

2.1. Preparation of decellularized cartilage ECM

Articular cartilage was isolated from fresh porcine hind knee joints. The cartilage tissue was frozen in liquid nitrogen and pulverized into a fine powder. Decellularization was performed according to a previously reported protocol with minor modifications [14]. Briefly, cartilage powder was treated with 2% sodium dodecyl sulfate (SDS) at 4 °C for 4 h, followed by washing in phosphate-buffered saline (PBS; pH 7.4) for 1 h. The samples were subsequently incubated in DNase I solution (200 U/mL; Sigma-Aldrich, St. Louis, MO, USA) for 4 h to remove residual nucleic acids. After a second PBS wash for 1 h, one complete decellularization cycle was achieved [20]. The procedure was repeated until a fully decellularized ECM was obtained. The decellularized ECM was then digested in pepsin solution (0.25 mg/mL) at 37 °C for 24 h, rinsed thoroughly with ultrapure water, and processed into a gel. The ECM gel was frozen at −80 °C and subsequently lyophilized to obtain ECM powder. The resulting powder was sterilized by irradiation and stored at −20 °C until further use.

2.2. Preparation of PCL scaffolds

PCL (Shanghai Yuanye Bio-Technology Co., Ltd., Shanghai, China) was used to fabricate 3D-printed scaffolds. Scaffold models were designed using SolidWorks 2016 with a thickness of 2.5 mm, a pore size of 0.9 mm, and a filament laydown angle of 90°. The digital models were imported into a fused deposition modeling (FDM) 3D printer, and porous PCL scaffolds with interconnected architectures were fabricated using optimized printing parameters. Following fabrication, all scaffolds were sterilized with ethylene oxide and stored at room temperature until use [22].

2.3. Surface functionalization of PCL scaffolds with E7 peptide

The BMSC-affinity peptide E7 (sequence: EPLQLKM; molecular weight: 858 Da) was commercially synthesized and purified to >95% purity (Scilight Peptide Inc., Beijing, China). Surface functionalization was performed using sulfosuccinimidyl 4-(N-maleimidomethyl) cyclohexane-1-carboxylate (sulfo-SMCC; Thermo Fisher Scientific, Rockford, IL, USA) as a heterobifunctional cross-linker. Briefly, pre-fabricated PCL scaffolds were immersed in 10 wt% 1,6-hexanediamine dissolved in isopropanol and incubated at 37 °C for 2 h to introduce surface amine groups. The scaffolds were then thoroughly rinsed with ultrapure water and washed with activation buffer (0.1 M PBS containing 0.15 M NaCl, pH 7.2). Subsequently, the scaffolds were incubated in sulfo-SMCC solution (2 mg/mL in PBS) for 1 h at room temperature. After activation, the scaffolds were washed with conjugation buffer (0.1 M PBS containing 0.1 M EDTA, pH 7.0) and incubated overnight at 4 °C in E7 peptide solution (2 mg/mL in conjugation buffer). The peptide-functionalized scaffolds were washed three times with ultrapure water to remove unbound peptide and stored at 4 °C until further use.

2.4. Preparation of ECM/E7-PCL composite scaffolds

ECM powder was dissolved in ultrapure water at a concentration of 20 mg/mL and homogenized using a high-speed homogenizer until a uniform suspension was obtained. The E7-modified PCL scaffolds were immersed in the ECM suspension and centrifuged at 8,000 × g for 5 min to facilitate ECM infiltration and deposition throughout the scaffold structure. The scaffolds were subsequently frozen at −80 °C for 2 h and lyophilized. To stabilize the ECM layer, the freeze-dried scaffolds were immersed in 70% (v/v) ethanol for 24 h to induce cross-linking. The scaffolds were then lyophilized again to obtain the final ECM/E7-PCL composite scaffolds [1,21].

2.5. Isolation, culture, and characterization of BMSCs

BMSCs were isolated from one-month-old male New Zealand White rabbits using Percoll density-gradient centrifugation as previously described [23]. Briefly, bone marrow was aspirated from the tibial and femoral medullary cavities using a bone marrow aspiration needle and layered onto lymphocyte separation medium for density-gradient centrifugation. The mononuclear cell fraction enriched with MSCs was collected, diluted with PBS, washed twice, and centrifuged at 1,000 × g for 10 min. The resulting cell pellet was resuspended in DMEM/F12 medium supplemented with 10% fetal bovine serum (FBS; Gibco, Grand Island, NY, USA) and 1% penicillin-streptomycin (PS; 100 U/mL penicillin and 100 μg/mL streptomycin). Cells were seeded into culture flasks and maintained under standard culture conditions. To verify their stem-cell characteristics, the isolated cells were subjected to trilineage differentiation assays, including adipogenic, osteogenic, and chondrogenic induction. In addition, flow cytometric analysis was performed to assess the expression of characteristic BMSC surface markers and confirm cell identity.

2.6. Scaffold characterization

2.6.1. Scanning electron microscopy (SEM)

The 3D-printed PCL, ECM/PCL (E/P), and ECM/E7-PCL (E/E7-P) scaffolds were freeze-dried and sputter-coated with gold prior to imaging. The surface morphology and microstructural features of the scaffolds were examined using a scanning electron microscope operated at an accelerating voltage of 15 kV. The average fiber diameter was quantified using ImageJ software (National Institutes of Health, Bethesda, MD, USA).

2.6.2. Fourier Transform Infrared (FTIR) spectroscopy

FTIR spectroscopy was performed to characterize the chemical composition of PCL and E7-PCL scaffolds. Spectra were acquired using a Nicolet Nexus 670 FTIR spectrometer (Thermo Fisher Scientific, Waltham, MA, USA) over a wavenumber range of 200–4000 cm^{-1} with a resolution of 2 cm^{-1}.

2.6.3. Pore size and porosity analysis

The pore morphology of the freeze-dried composite scaffolds was examined by SEM. Scaffold porosity was determined using the ethanol displacement method. Briefly, the initial volume of

ethanol was recorded as V_0. After immersion of the scaffold in ethanol for 5 min, the total volume was recorded as V_1. Following removal of the scaffold, the remaining ethanol volume was recorded as V_2. The porosity of scaffolds was calculated using the following formula: $(V_0-V_2)/(V_1-V_2) \times 100\%$. All measurements were performed in triplicate.

2.6.4. Mechanical testing

Prior to mechanical testing, scaffolds were immersed in PBS at 37 °C for 1 h to achieve equilibrium hydration. Excess surface moisture was gently removed using filter paper. Cylindrical specimens (diameter: 5 mm; height: 4 mm) were subjected to uniaxial compression using a universal testing machine (Zwick Z020, Germany). Compression was applied at a displacement rate of 0.5 mm/min until a maximum strain of 10% was reached, followed by complete unloading. This loading-unloading cycle was repeated 2-5 times to precondition the samples. The compressive modulus was determined from the initial linear region of the stress-strain curve [25]. All measurements were performed in triplicate.

2.6.5. Water absorption capacity

The water absorption capacities of PCL, E/P, and E/E7-P scaffolds were evaluated. The initial dry weight of each scaffold was recorded as W_0. Samples were immersed in deionized water, and wet weights (W_t) were measured after 2, 4, 6, and 8 min. Prior to weighing, excess surface water was gently removed using filter paper. The water absorption rate was calculated using the following equation: $(W_t-W_0)/W_0 \times 100\%$ [24], where W_t is the wet weight at time t. All measurements were performed in triplicate.

2.7. Quantification of type II collagen and GAG contents in ECM

The collagen content retained in the decellularized ECM was quantified using a Sircol™ Insoluble Collagen Assay Kit (Biocolor, Carrickfergus, UK). Briefly, 20 mg of ECM powder was mixed with pepsin solution (0.5 M acetic acid) at a ratio of 1:50 (w/v) and incubated at 37 °C for 18 h, with vortexing every 30 min to facilitate digestion. The resulting suspension was transferred to a 2 mL centrifuge tube, and dissociation reagent was added at a ratio of 20:1 (w/v) relative to the ECM. Samples were subsequently incubated at 65 °C for 3 h with intermittent vortexing every 30 min. Following centrifugation at 12,000 rpm for 10 min, the supernatant was collected for analysis.

A standard curve was generated using hydrolyzed bovine collagen standards. Samples and standards were added to a 96-well plate, and absorbance was measured at 550 nm using a microplate reader. Collagen concentrations were calculated from the standard curve. All measurements were performed in triplicate.

The GAG content of the ECM was determined using the dimethylmethylene blue (DMB) assay [24]. Briefly, approximately 50 mg of each sample was digested in 1 mL of papain digestion buffer (100 mM sodium phosphate, 10 mM EDTA, 10 mM cysteine-HCl, pH 6.5) containing 125 μg/mL papain. Samples were incubated at 60 °C for 24-72 h until complete digestion was achieved. The digested samples were centrifuged at 10,000 × g for 5 min, and 100 μL of the supernatant was mixed with 3 mL of DMMB reagent. Absorbance was measured at 480 nm using a UV-visible spectrophotometer. GAG concentrations were determined from a standard calibration curve and expressed as micrograms of GAG per milligram of dry ECM:

$$\text{Hydroxyproline (μg/mL)} = \frac{(A_{sample}\text{-}A_{blank})}{(A_{standard}\text{-}A_{blank})} \times \text{hydroxyproline concentration in the standard (μg/mL)} \times \frac{\text{10 mL total hydrolysate volume}}{\text{tissue wet weight (mg)}}$$

(A_{sample} is the absorbance of the sample, A_{blank} is the absorbance of the blank, and $A_{standard}$ is the absorbance of the standard).

2.8. Cytotoxicity and cell proliferation assays

To evaluate the biocompatibility of the scaffolds, BMSCs were seeded onto E/P and E/E7-P composite scaffolds at a density of 5×10^5 cells per scaffold. After allowing 3 h for cell attachment, the cell-seeded scaffolds were cultured in DMEM supplemented with 10% FBS and 1% PS. BMSCs cultured under standard conditions without scaffolds served as the control group. Cell viability and proliferation were assessed after 1, 3, and 5 days of culture using a Live/Dead viability assay and a Cell Counting Kit-8 (CCK-8; Dojindo, Kumamoto, Japan), respectively. For the CCK-8 assay, absorbance was measured at 450 nm using a microplate reader.

2.9. Quantitative reverse transcription polymerase chain reaction (qRT-PCR)

To evaluate chondrogenic differentiation, second-passage BMSCs were seeded onto E7-P and E/E7-P composite scaffolds at a density of 2×10^7 cells per scaffold according to a previously

reported protocol [26]. Following 4 h of cell attachment, the constructs were cultured in standard growth medium. BMSCs cultured under standard conditions without scaffolds served as the control group. After 7 and 14 days of culture, total RNA was extracted using TRIzol reagent (TaKaRa, Shiga, Japan) according to the manufacturer's instructions. Complementary DNA (cDNA) was synthesized and subjected to qRT-PCR using a LightCycler® 480 II system (Roche Diagnostics Ltd., Shanghai, China). The expression levels of cartilage-related genes, including SOX9, COL2A1, superficial zone protein (SZP), and aggrecan (ACAN), were analyzed. β-Actin was used as the internal reference gene. Relative gene expression levels were calculated using the $2^{-\Delta\Delta Ct}$ method. Primer sequences are listed in **Table 1**. The PCR cycling conditions consisted of an initial denaturation step at 95 ℃ for 5 min, followed by 35 cycles of denaturation at 95 ℃ for 15 s, annealing at 55 ℃ for 30 s, and extension at 72 ℃ for 30 s.

Table 1. Primer sequences.

Gene	Primers	
	Forward (5'-3')	**Reverse (5'-3')**
ACAN	TCGAGGACAGCGAGGCC	TCGAGGGTGTAGCGTGTAGAGA
Collagen II	AGCCTGGTGTCATGGGTTTC	GTCCCTTCTCACCAGCTTTGC
SOX9	CCCCAACAGATCGCCTACAGT	GAGTTCTGGTGGTCGGTGTAGTC
SZP	TTGCTCCTGGTGCTGCTG	GCTGATGGTGGTGATGGTG

2.10. Immunofluorescence staining

To detect the expression of cartilage-specific proteins, BMSCs were seeded onto the composite scaffolds and cultured in chondrogenic differentiation medium for 21 days. The constructs were gently washed with PBS, fixed with 4% paraformaldehyde for 30 min, permeabilized with 0.5% Triton X-100 for 15 min, and blocked with 5% bovine serum albumin (BSA) for 1 h at room temperaturem Samples were subsequently incubated overnight at 4 °C with primary antibodies against SZP (MABT400, Merck, Darmstadt, Germany) and aggrecan (MA3-16888, Invitrogen, Carlsbad, CA, USA) at a concentration of 6 μg/mL [27]. After washing with PBS, the constructs were incubated with a Cy3-conjugated goat anti-mouse IgG secondary antibody (AB97035, Abcam, Cambridge, UK) for 1 h at room temperature. The actin cytoskeleton was stained with

FITC-phalloidin (Shanghai Biotics Co., Ltd., Shanghai, China), and cell nuclei were counterstained with 4′,6-diamidino-2-phenylindole (DAPI; Invitrogen, Carlsbad, CA, USA). Fluorescence images were acquired using a confocal laser scanning microscope (CLSM).

2.11. *In vivo* animal study

Twenty-four healthy male New Zealand White rabbits (4 months old, 2.5-3.0 kg) were used in this study. All experimental procedures were approved by the Animal Care and Use Committee of Beijing Vital River Laboratory Animal Technology Co., Ltd. (Approval No. AWE2022060305). Animals were randomly assigned to three groups (n = 8 per group): control, E/P, and E/E7-P. General anesthesia was induced by intravenous injection of 3% pentobarbital sodium (30 mg/kg) via the marginal ear vein. The right knee joint was exposed through a medial parapatellar approach, and a full-thickness osteochondral defect (4 mm in diameter × 4 mm in depth) was created in the center of the femoral trochlear groove. Subsequently, three to four microfracture holes (1 mm in diameter and 5 mm in depth) were created in the subchondral bone using a 1-mm Kirschner wire. Composite scaffolds were press-fitted into the defects in the E/P and E/E7-P groups, whereas defects in the control group were left untreated. Animals were sacrificed at 6 and 12 weeks postoperatively, and repaired tissues were harvested for evaluation. Cartilage repair outcomes were assessed using the International Cartilage Regeneration & Joint Preservation Society (ICRS) scoring system [28].

2.12. Gross observation, MRI imaging, and histological assessment

Macroscopic evaluation of cartilage repair was independently performed by two blinded observers using the ICRS macroscopic assessment scale. MRI was conducted to assess tissue regeneration within the defect area and the restoration of the articular surface. MRI parameters were as follows: zoom factor = 1.58, field strength = 3.0 T, slice thickness = 0.5 mm, repetition time (TR) = 26.0 ms, and echo time (TE) = 4.9 ms [29]. Following MRI examination, osteochondral specimens were harvested, fixed, decalcified, embedded, and sectioned for histological analysis. Tissue sections were stained with Safranin O/Fast Green, toluidine blue, and other cartilage-specific histological stains to evaluate matrix deposition and tissue morphology. Collagen-specific staining was also performed to assess the quality of regenerated cartilage.

2.13. Statistical analysis

All quantitative data are presented as mean ± standard deviation (SD). Statistical analyses were performed using SPSS version 20.0 (IBM Corp., Armonk, NY, USA). Comparisons among multiple groups were conducted using one-way analysis of variance (ANOVA), followed by Tukey's post hoc test for pairwise comparisons. Differences were considered statistically significant at $P < 0.05$ and highly significant at $P < 0.01$.

3. Results

3.1. Morphology of the composite scaffolds

The fabrication process of the E7 peptide-modified PCL scaffold is illustrated in **Figure 2A**. Representative images of the 3D-printed PCL scaffold are shown in **Figure 2B**, demonstrating a well-defined architecture with interconnected porous networks generated using optimized printing parameters. SEM observations and FTIR analysis confirmed the successful incorporation of ECM and E7 peptide onto the PCL scaffold (**Figure A1** and **Figure 2C**). The resulting E/E7-P composite scaffold exhibited a biphasic structure in which both the PCL framework and ECM layer retained their characteristic morphological features. No obvious interfacial separation or structural discontinuity was observed between the two phases, indicating effective integration and stable interfacial bonding. Such structural continuity is advantageous for maintaining scaffold integrity during tissue regeneration and may facilitate the coordinated regeneration of cartilage and subchondral bone tissues.

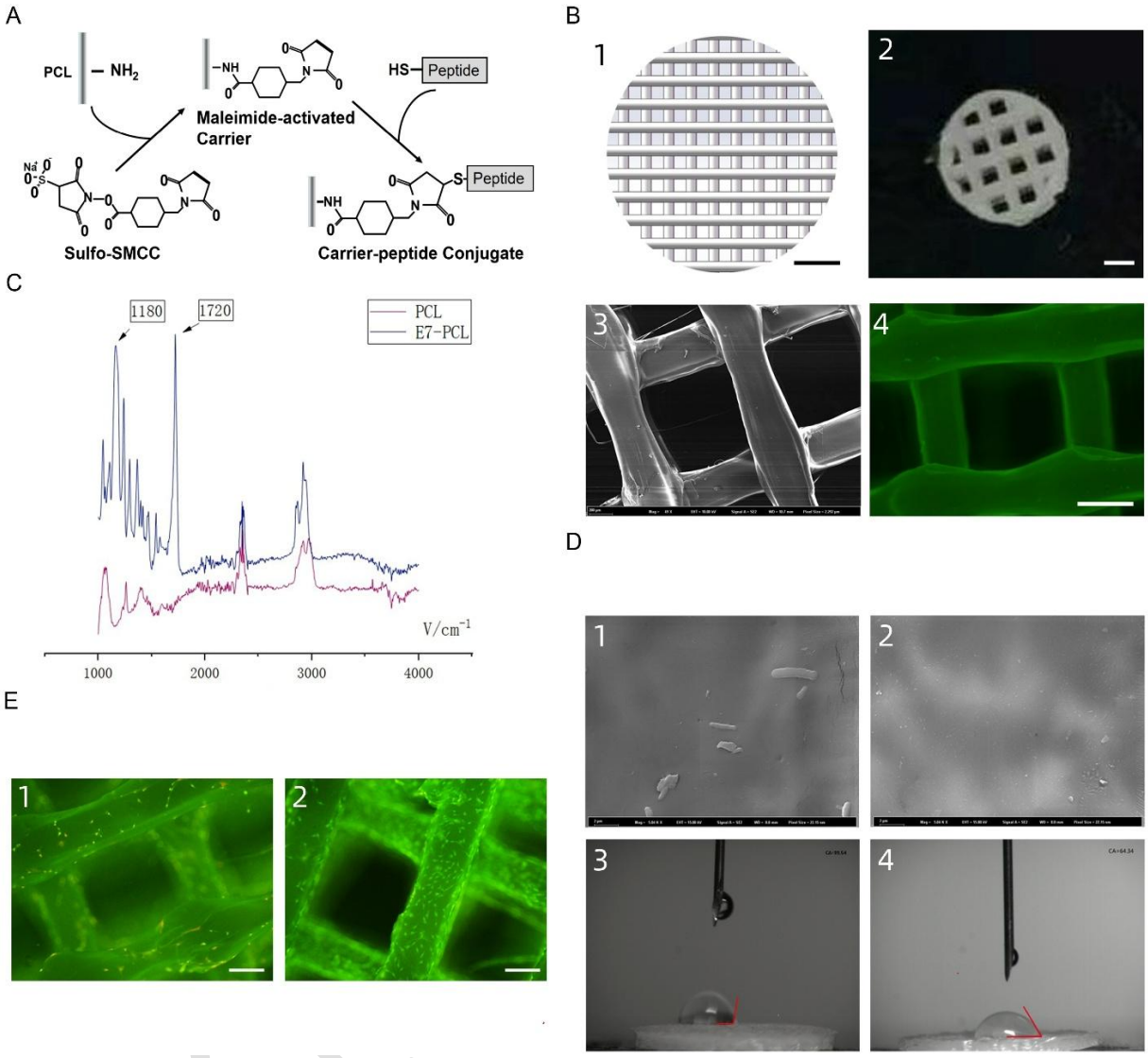

Figure 2. Characterization of E7 peptide-modified PCL scaffolds

A. Schematic illustration of the covalent conjugation of FITC-labeled peptides onto PCL scaffolds using sulfo-SMCC as the crosslinker between the FITC-tagged peptide and the electrospun PCL fibers. **B.** Characterization of 3D-printed PCL scaffolds: (1) 3D structural design (scale bar = 2 mm); (2) macroscopic image (scale bar = 1 mm); (3) SEM micrographs of PCL fibers (scale bar = 500 μm); (4) fluorescence microscopy image demonstrating successful conjugation of FITC-labeled E7 peptide (scale bar = 500 μm). **C.** Fourier transform infrared (FTIR) spectra of pure PCL and E7-P scaffolds. **D.** Surface morphology and hydrophilicity characterization: (1) SEM image of pure PCL and scaffold surface; (2) SEM image of E7-P scaffold surface; (3) water contact angle of pure PCL scaffold; (4) water contact angle of E7-PCL scaffold. **E.** Cytoskeleton fluorescence staining of BMSCs cultured on scaffolds (FITC-phalloidin, scale bar = 500 μm): (1) pure PCL scaffold; (2) E7-P scaffold.

3.2. Characterization of the composite scaffolds

Macroscopic observation revealed that the E/E7-P composite scaffold possessed a uniform white appearance and a highly porous three-dimensional structure (**Figure 3A**). SEM analysis further demonstrated the presence of interconnected pores distributed throughout the scaffold (**Figure 3B**). Consistently, fluorescence imaging of BMSCs cultured within the scaffold confirmed homogeneous cellular distribution and infiltration across the porous network (**Figure 3C**). The highly interconnected architecture is favorable for nutrient transport, cellular infiltration, waste exchange, and extracellular matrix deposition, all of which are essential for successful tissue regeneration. Previous studies have shown that scaffold pore size can influence stem-cell fate by modulating cellular morphology and the local microenvironment. Smaller pores tend to favor chondrogenic differentiation by promoting cell aggregation and creating a relatively hypoxic niche, whereas larger pores are generally more conducive to vascularization and osteogenic differentiation. Accordingly, the pore architecture of the present scaffold may provide a suitable microenvironment for supporting cartilage regeneration. To evaluate the quality of the decellularized ECM, residual DNA, collagen II, and GAG contents were quantified. As shown in **Figure 3D-F**, the decellularization process effectively removed cellular components while preserving key cartilage-specific ECM constituents, including collagen II and GAGs. These results indicate that the prepared ECM retained its essential biological composition and is therefore suitable for cartilage tissue-engineering applications. Taken together, these findings demonstrate that the composite scaffold possesses a highly porous architecture, favorable structural characteristics, and a biologically active ECM component capable of supporting cell attachment and tissue regeneration.

3.3. Water absorption capacity of the composite scaffolds

The water absorption behavior of pure PCL and E/E7-P composite scaffolds is shown in **Figure 3G**. Water uptake is an important property of tissue-engineered scaffolds because it influences nutrient transport, biomolecule retention, and cellular activity within the construct [30]. Compared with pure PCL, the E/E7-P scaffold exhibited significantly enhanced water absorption capacity ($P < 0.05$). The water absorption ratio of the E/E7-P scaffold increased rapidly over time and reached approximately 315% after 8 min of immersion, and remained stable at this plateau for an extended period thereafter; accordingly, we recorded the water absorption changes within 8 min for

immersion to capture the rapid hydration phase of the scaffolds. In contrast, pure PCL displayed substantially lower water uptake. The enhanced hydrophilicity of the composite scaffold is likely attributable to the incorporation of ECM components, which contain abundant hydrophilic functional groups capable of retaining water molecules. The improved water absorption capacity may contribute to the maintenance of a hydrated microenvironment that supports cell adhesion, survival, proliferation, and matrix deposition, thereby facilitating cartilage regeneration.

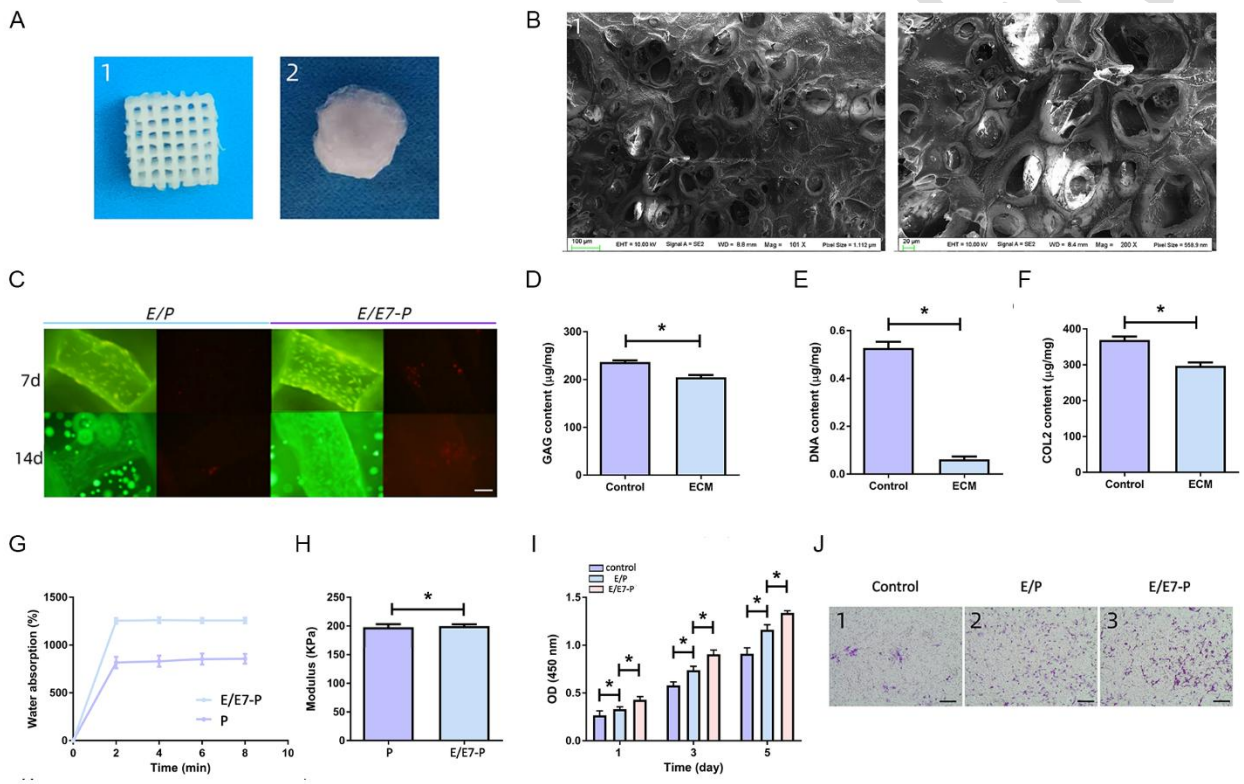

Figure 3. Physicochemical characterization of E/E7-P composite scaffolds and their *in vitro* biological properties

A. Macroscopic appearance: (1) pure PCL scaffold; (2) E/E7-P composite scaffold. **B.** SEM images showing the surface morphology of E/E7-P composite scaffold. **C.** Live/dead fluorescent staining images of BMSCs seeded on E/P and E/E7-P scaffolds after 7 and 14 days of culture (scale bar = 100 μm). **D.** Quantification of glycosaminoglycan (GAG) content in the ECM. **E.** Assessment of residual DNA content in the ECM. **F.** Collagen II content in the ECM. **G.** Water absorption kinetics of pure PCL (P) and E/E7-P scaffolds. **H.** Compressive modulus of pure PCL (P) and E/E7-P scaffolds. **I.** CCK-8 assay for cell proliferation of BMSCs cultured on control, E/P, and E/E7-P scaffolds for 1, 3, and 5 days. **J.** Transwell-

migration images after 24 h of incubation. Optical microscopy images of BMSC migration in control, E/P, and E/E7-P groups (scale bar = 200 μm). *P < 0.05.

3.4. Mechanical properties of the composite scaffolds

The compressive mechanical properties of pure PCL and E/E7-P scaffolds are presented in **Figure 3H**. Mechanical performance is a critical consideration in scaffold design because the mechanical microenvironment can influence stem-cell behavior and tissue regeneration. Compression testing demonstrated that the composite scaffold maintained favorable mechanical strength despite the incorporation of ECM. The PCL framework provided structural stability and load-bearing capacity, whereas the ECM component contributed biological functionality without substantially compromising the overall integrity of the scaffold. The resulting mechanical properties are expected to provide adequate support for defect repair while maintaining a microenvironment conducive to cellular activity. Previous studies have shown that substrate stiffness can regulate mesenchymal stem-cell differentiation through mechanotransduction pathways. In the present scaffold system, the mechanically robust PCL framework may contribute to structural support and subchondral bone repair, whereas the ECM-rich microenvironment provides biological cues favorable for chondrogenic differentiation and cartilage-specific matrix synthesis.

3.5. Cell survival, adhesion, and recruitment on composite scaffolds

An ideal scaffold for cartilage tissue engineering should provide a favorable microenvironment for cell attachment, survival, and proliferation. To evaluate the cytocompatibility of the composite scaffolds, BMSCs were seeded onto E/P and E/E7-P scaffolds and cultured for up to 5 days. Live/Dead staining and CCK-8 assays demonstrated high cell viability and sustained proliferation in both groups throughout the culture period (**Figure 3I**), indicating that neither scaffold exhibited detectable cytotoxicity. Although no significant differences in overall cell viability were observed between groups, the E/E7-P scaffold consistently showed enhanced initial cell attachment compared with the E/P scaffold. Transwell migration assays further demonstrated that the E7-modified scaffold possessed a greater capacity to recruit BMSCs under identical culture conditions (**Figure 3J**). In addition, fluorescence imaging revealed that BMSCs were uniformly distributed throughout the porous scaffold architecture and exhibited normal cellular morphology.

3.6. *In vitro* chondrogenic differentiation assessed by immunofluorescence and qRT-PCR

The ability of the composite scaffolds to promote chondrogenic differentiation was evaluated by immunofluorescence staining and qRT-PCR. Immunofluorescence analysis demonstrated positive expression of SZP and ACAN in both the E/P and E/E7-P groups (**Figure 4A-F**). Notably, the E/E7-P scaffold exhibited stronger fluorescence intensity for both markers, suggesting enhanced chondrogenic matrix production following incorporation of the E7 peptide and cartilage-derived ECM. Consistent with the immunofluorescence results, qRT-PCR analysis revealed significant upregulation of cartilage-related genes, including *SOX9*, *SZP*, and *ACAN*, in the scaffold-treated groups compared with the control group (**Figure 4G-I** and **5A-C**). Gene expression levels were normalized to those of control BMSCs at day 0. Both the E/P and E/E7-P groups exhibited a time-dependent increase in chondrogenic gene expression during the culture period. The expression of key chondrogenic markers progressively increased and reached maximal levels at day 14. Subsequently, expression levels gradually declined by day 21, a pattern consistent with the progression of chondrogenic differentiation and matrix maturation.

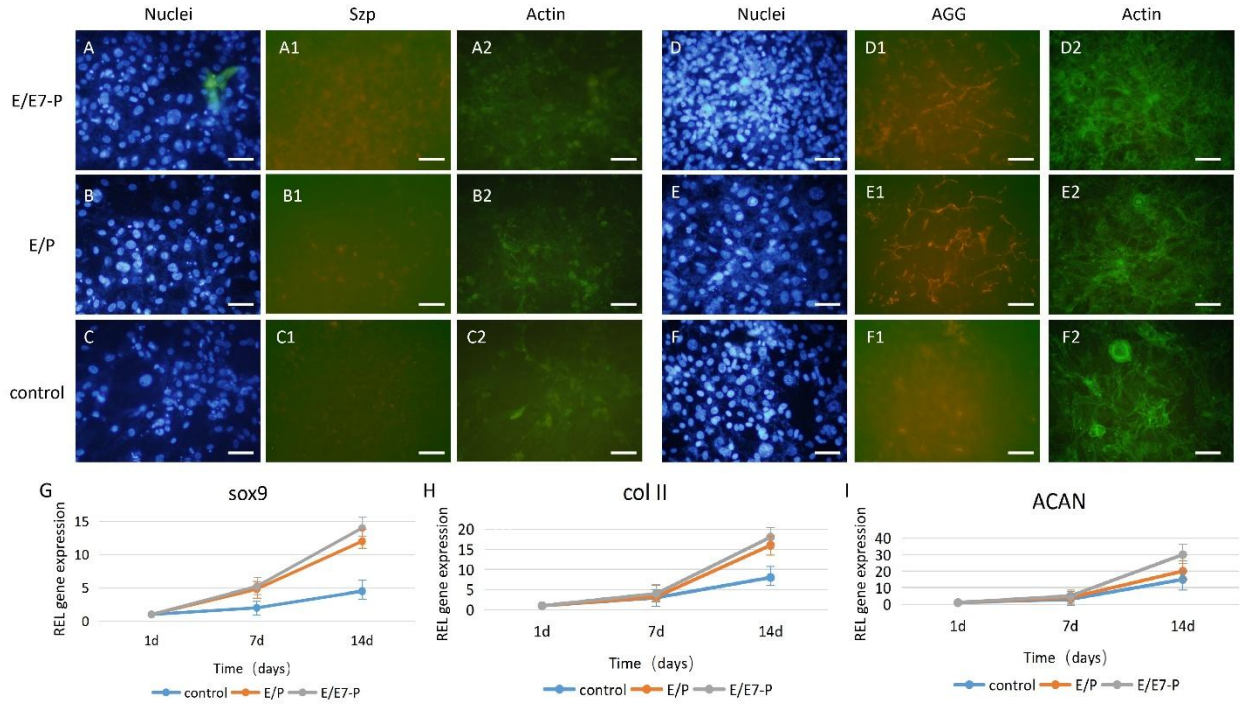

Figure 4. *In vitro* chondrogenic differentiation of BMSCs on composite scaffolds

A–F. Immunofluorescence staining showing the expression of SZP and AGG in the composite scaffolds (E/P and E/E7-P groups) after 14 days of induction (scale bar = 100 μm). G**–I.** RT-PCR analysis of chondrogenic gene expression at 1, 7, and 14 days.

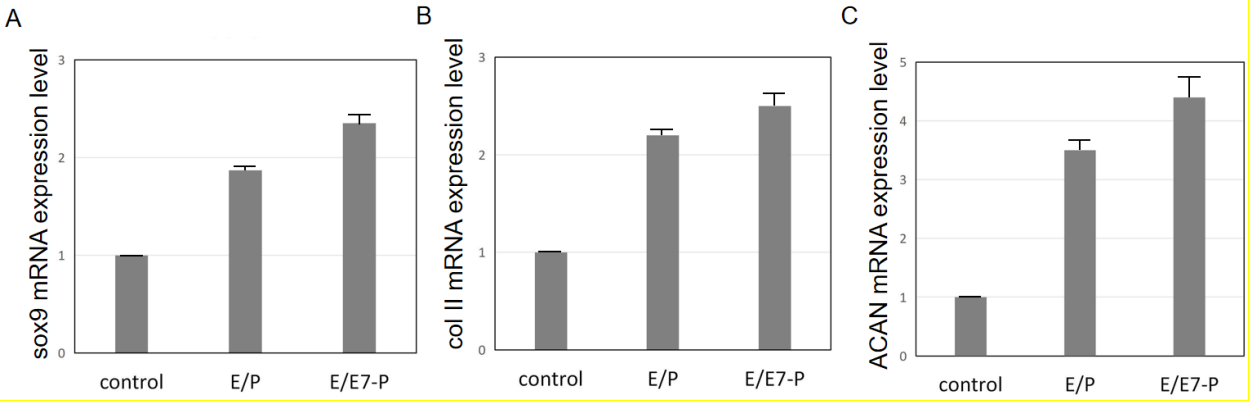

Figure 5. Relative mRNA expression of chondrogenic (Sox9, Col II, ACAN) and catabolic (Mmp13) genes determined by RT-qPCR. All data were normalized to GAPDH via the 2^−ΔΔCt method, with the Ctrl group normalized to 1. Values are presented as mean ± SEM, n = 4 biological replicates. Statistical analysis was performed using one-way ANOVA with Tukey's multiple comparison test.

3.7. *In vivo* assessment of chondrogenic regeneration

The cartilage repair performance of the composite scaffolds was assessed using gross observation, ICRS scoring, MRI, and histological analyses. At 6 weeks after implantation, defects in the untreated control group remained obviously visible, exhibiting distinct boundaries from the surrounding native cartilage and obvious surface depression (**Figure 6A** and **Table 2**). In contrast, both scaffold-treated groups displayed newly formed cartilage-like tissue within the defect area. Quantitative ICRS assessment demonstrated significantly higher repair scores in the E/E7-P group than in the E/P and control groups ($P < 0.05$; **Figure 6B**), indicating enhanced early-stage cartilage regeneration. MRI findings were consistent with the macroscopic observations (**Figure 6C**). At 6 weeks, the E/E7-P group exhibited more extensive defect filling and greater tissue thickness than the E/P and control groups. The regenerated tissue in the E/E7-P group also displayed imaging characteristics more closely resembling those of native cartilage. At 12 weeks, defects in the control group remained readily identifiable and were predominantly filled with fibrous or fibrocartilaginous repair tissue. In contrast, both scaffold-treated groups showed substantial restoration of the articular surface. Although a slight surface depression remained in the E/P group, the E/E7-P group exhibited nearly complete restoration of the defect region with a smooth and continuous articular surface. Histological analyses further confirmed the superior regenerative performance of the E/E7-P scaffold (**Figure 7**). At 6 weeks, the E/E7-P group displayed more

abundant and thicker cartilage-like tissue formation than the E/P group (**Figure 7A-C**). By 12 weeks, the defect area in the E/E7-P group was almost completely filled with hyaline cartilage-like tissue exhibiting structural characteristics comparable to those of native articular cartilage (**Figure 7D-F**). The interface between regenerated and surrounding cartilage was largely indistinguishable, and a well-defined tidemark was observed, indicating successful integration with the underlying subchondral bone.

Table 2. Macroscopic and histological scores of femoral trochlear cartilage defect repair in control group, E/P group, and E/E7-P group.

Group	**ICRS score**	**MOHS score**
Control Group 6W	2.83 ± 0.37	3.67 ± 1.97
Control Group 12W	3.33 ± 0.47	5.50 ± 0.96
E/P Group 6W	4.65 ± 0.53	5.75 ± 1.54
E/P Group 12W	7.23 ± 0.66	9.62 ± 0.85
E/E7-P Group 6W	8.00 ± 0.81	16.17 ± 1.57
E/E7-P Group 12W	10.67 ± 0.75	21.83 ± 1.86

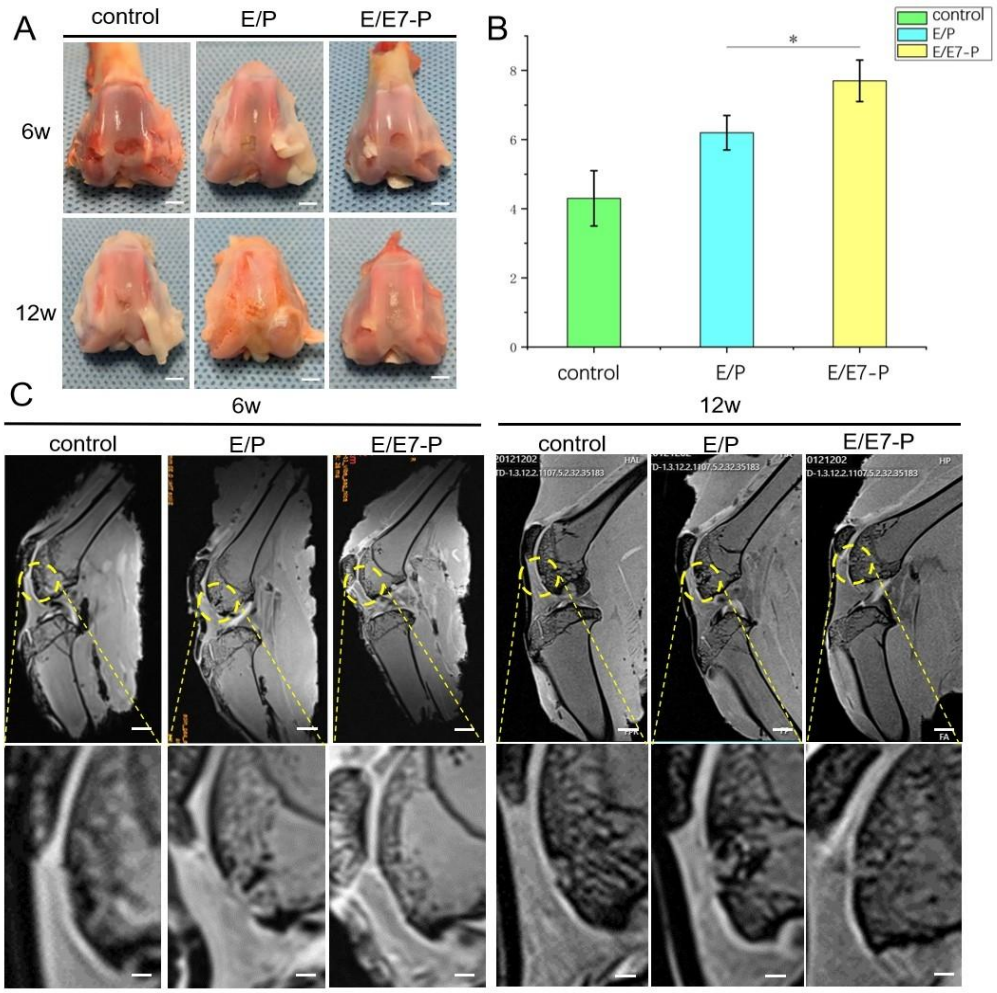

Figure 6. Gross observation, ICRS scoring and MRI evaluation of cartilage repair at 6 and 12 weeks postoperatively

A. Macroscopic appearance of repaired cartilage in control, E/P and E/E7-P groups at 6 and 12 weeks (Scale bar = 5 mm). **B.** ICRS macroscopic scores of cartilage repair in each group at 12 weeks. *P < 0.05. **C.** MRI evaluation of the repaired cartilage at 6 and 12 weeks. The yellow dashed circles indicate the defect sites (scale bar = 5 mm for full-view images, scale bar = 2 mm for magnified images).

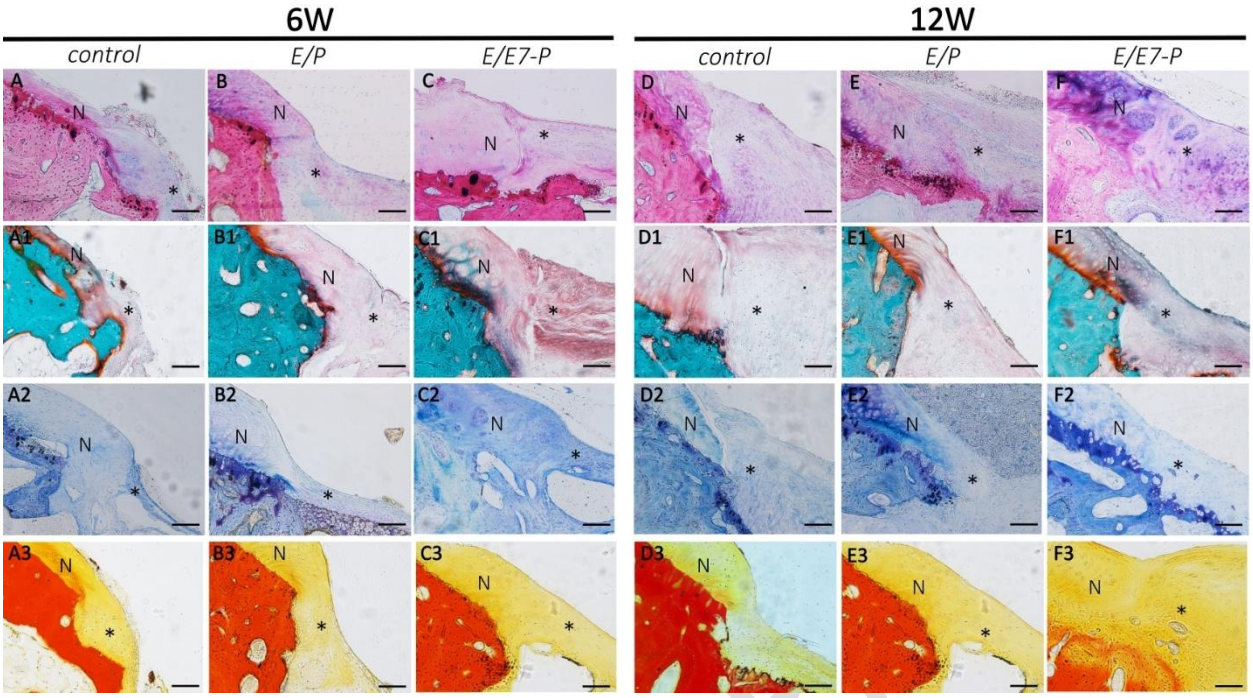

Figure 7. Histological evaluation of cartilage repair at 6 and 12 weeks postoperatively

Hard-tissue histological staining of the cartilage defect regions in the control, E/P, and E/E7-P groups at 6 weeks (**A–C)** and 12 weeks **(D–F)** postoperatively, including H&E staining, Safranin O/Fast Green staining, toluidine blue staining, and ACAN immunostaining. *N* indicates native cartilage, and asterisks (*) mark the original defect sites. Scale bar = 200 μm).

4. Discussion

In the present study, we developed a biomimetic ternary composite scaffold consisting of cartilage-derived ECM, an E7 BMSC-affinity peptide, and a 3D-printed PCL framework for the repair of articular cartilage defects. The scaffold was systematically characterized in terms of its physicochemical properties, cytocompatibility, and cartilage-regenerative capacity both *in vitro* and *in vivo*. Our findings demonstrate that the integration of these three functional components generates a synergistic regenerative platform that combines mechanical support, targeted stem-cell recruitment, and biomimetic biochemical signaling. This multifunctional design addresses several key limitations of conventional scaffold systems and provides a promising strategy for acellular cartilage tissue engineering.

PCL has been widely used as a structural material for cartilage tissue engineering owing to its excellent processability, favorable biocompatibility, and tunable mechanical properties. However,

the hydrophobic nature of PCL and its lack of intrinsic biological recognition sites limit cellular attachment, migration, and differentiation. Consequently, pure PCL scaffolds often exhibit insufficient bioactivity to effectively support cartilage regeneration, resulting in the formation of fibrocartilaginous repair tissue rather than mechanically competent hyaline cartilage-like tissue [31,32]. To overcome these limitations, we introduced E7 affinity peptides and cartilage-derived ECM into the PCL scaffold. Covalent immobilization of the E7 peptide significantly enhanced BMSC adhesion and recruitment, while ECM incorporation provided a biologically relevant microenvironment enriched with cartilage-specific matrix components, including collagens and glycosaminoglycans. The *in vitro* results support this synergistic effect. Compared with unmodified PCL, the composite scaffold promoted greater cell attachment and proliferation and significantly enhanced the expression of chondrogenic markers, including COL2A1, ACAN, and SOX9. These findings are consistent with previous studies demonstrating that affinity-peptide functionalization can improve stem-cell targeting and retention while preserving the chondrogenic phenotype [26]. Moreover, the ECM component provided structural and biochemical cues that closely mimic the native cartilage microenvironment, thereby facilitating extracellular matrix synthesis and cartilage-specific differentiation [33]. However, these in vitro findings cannot be directly extrapolated to the complex in vivo joint microenvironment.

Rather than acting independently, the peptide and ECM components appear to function cooperatively: E7-mediated recruitment increases the availability of reparative cells at the defect site, whereas the ECM provides the biological signals required to direct their differentiation toward a chondrogenic lineage. Among the various mesenchymal stem-cell populations investigated for cartilage regeneration, BMSCs remain one of the most extensively studied owing to their robust proliferative capacity, multilineage differentiation potential, and accessibility. Increasing attention has therefore been directed toward strategies that recruit endogenous BMSCs rather than relying on *ex vivo* cell expansion and transplantation [34]. Although endogenous BMSCs can migrate toward sites of injury, their regenerative contribution is often limited by poor cell retention, insufficient homing efficiency, and an unfavorable local microenvironment. As a result, endogenous cell recruitment represents an attractive alternative to conventional cell-based therapies because it reduces manufacturing complexity, lowers treatment costs, minimizes immunological concerns, and avoids regulatory challenges associated with cell transplantation [27]. The success of such approaches depends largely on the ability of biomaterials to actively recruit, retain, and regulate

endogenous progenitor cells. Accordingly, the development of scaffolds that simultaneously provide structural support and biological guidance represents an important direction in cartilage tissue engineering [28].

The structural characteristics of the scaffold also contributed substantially to its regenerative performance. An interconnected porous architecture is essential for facilitating nutrient transport, waste removal, cell migration, and matrix deposition within engineered cartilage constructs [32]. The 3D-printed PCL framework used in this study maintained a well-defined porous structure and adequate compressive strength, thereby providing mechanical stability during the early stages of tissue repair [35]. Meanwhile, incorporation of cartilage-derived ECM increased scaffold hydrophilicity and water-retention capacity, creating a more favorable microenvironment for cell survival and matrix production [36]. The enhanced water absorption observed in the E/E7-P scaffold may further promote the retention of endogenous cells and bioactive molecules within the defect site. Importantly, the addition of E7 affinity peptides significantly improved BMSC recruitment compared with the ECM/PCL scaffold alone, suggesting that selective cell targeting is a critical determinant of scaffold performance. Notably, although E7 affinity peptides significantly enhanced BMSC recruitment in vitro, whether this effect translates into improved endogenous stem cell homing and retention within cartilage defects in vivo remains to be established.

In vivo evaluation demonstrated that, by 12 weeks postoperatively, defects treated with the E/E7-P composite scaffold were largely filled with hyaline cartilage-like tissue. Histological analyses revealed significantly higher repair scores in the E/E7-P group than in the control and E/P groups, and the regenerated tissue exhibited good integration with the surrounding native cartilage without evidence of adverse inflammatory responses. In the in vivo experiments, to better preserve the structural integrity of the regenerated cartilage, we performed histological staining using resin-embedded hard tissue sections, in which the regenerated region was hardened with resin prior to staining. Compared with conventional paraffin sections, hard tissue sections have inherent limitations in staining contrast and detail presentation. Nevertheless, the staining results still provide valid histological evidence to support that the composite scaffold is conducive to cartilage tissue regeneration and repair. In follow-up studies, we will further optimize the tissue decalcification, embedding and staining procedures to improve staining quality and more clearly visualize the components and structure of the regenerated tissue. Consistent findings from gross

observation, MRI, and histological assessments collectively indicated that the E/E7-P scaffold achieved superior cartilage repair compared with both untreated defects and ECM/PCL scaffolds. It should be noted that these in vivo results are limited to young, healthy rabbits, and the repair efficacy of the scaffold in aged osteoarthritis pathological models has not been evaluated. Of note, although the regenerated cartilage shared high similarity with native articular cartilage, morphological gaps still existed compared with intact hyaline cartilage. This discrepancy is most likely associated with the observation duration, as the formation of fully normal hyaline cartilage requires extended periods of regeneration and tissue remodeling, which aligns with the inherently low regenerative capacity of articular cartilage. These results suggest that the synergistic combination of mechanical support, targeted stem-cell recruitment, and ECM-derived biological cues effectively overcomes several limitations associated with spontaneous cartilage healing and enhances the quality of tissue regeneration [37]. Unlike conventional cell-based therapies that require exogenous cell isolation, expansion, and transplantation, the present strategy relies on the recruitment and regulation of endogenous stem cells. This approach eliminates many of the challenges associated with cell manufacturing, including contamination risks, phenotypic instability during *in vitro* expansion, immunological concerns, and regulatory complexity. Consequently, endogenous regeneration-based therapies may offer advantages in terms of procedural simplicity, scalability, and clinical feasibility [38].

Despite these encouraging findings, several limitations should be acknowledged. Although the E7 affinity peptide significantly enhanced endogenous stem-cell recruitment, its grafting density, spatial distribution, and long-term stability were not systematically investigated. Future studies should optimize peptide immobilization strategies and clarify how peptide density and surface presentation influence biological performance. In addition, while the decellularized cartilage ECM retained key matrix components, further standardization of the decellularization and purification procedures is required to improve batch-to-batch consistency and ensure rigorous control of residual nucleic acids and antigenicity. From a translational perspective, the rabbit osteochondral defect model cannot fully reproduce the mechanical loading conditions, defect dimensions, and long-term repair processes of human joints. Moreover, although the PCL framework provided adequate structural support in the present study, its mechanical properties may be insufficient for high-load-bearing applications, highlighting the need for composite or hybrid biomaterials with improved mechanical performance while preserving favorable bioactivity. Methodologically,

long-term scaffold degradation, degradation-associated immune responses, and the dynamic processes of cell behavior and tissue remodeling were not systematically monitored, limiting the evaluation of long-term biosafety and regenerative mechanisms. Furthermore, matrix characterization relied primarily on biochemical assays and semi-quantitative histological analyses, whereas advanced techniques such as spatial proteomics or Raman spectroscopy were not employed to assess the spatial heterogeneity and compositional maturation of regenerated cartilage. Finally, the biological performance of the scaffold was evaluated only using rabbit BMSCs under standard culture conditions without multicellular co-culture systems or osteoarthritis-related inflammatory stimulation, leaving its regenerative potential in the complex pathological joint microenvironment to be further established. Collectively, addressing these limitations will facilitate the optimization of scaffold design and provide a stronger foundation for future clinical translation.

5. Conclusion

In this study, we developed a biomimetic composite scaffold comprising a 3D-printed PCL framework, an E7 BMSC-affinity peptide, and cartilage-derived ECM for articular cartilage regeneration. Functionalization with the E7 peptide enhanced the biological activity of the scaffold and significantly improved its ability to recruit and retain BMSCs. The incorporation of cartilage-derived ECM further provided a biomimetic microenvironment that supported cell adhesion, chondrogenic differentiation, and extracellular matrix deposition. The resulting composite scaffold exhibited favorable mechanical properties, excellent biocompatibility, and enhanced regenerative potential both *in vitro* and *in vivo*. Importantly, implantation of the E/E7-P scaffold promoted the formation of well-integrated hyaline cartilage-like tissue and achieved superior repair outcomes compared with control treatments. Within the scope of the current data and its inherent experimental limitations, these findings demonstrate that the combined strategy of mechanical stabilization, targeted endogenous stem-cell recruitment, and ECM-mediated biological induction represents an effective approach for cartilage regeneration.

Acknowledgments

None.

Funding

This research did not receive any specific grant from funding agencies in the public, commercial, or not-for-profit sectors.

Conflict of interest

The authors declare they have no competing interests.

Author contributions

Conceptualization: Xinqiang Zhao
Data curation: Xinqiang Zhao, Xiaoning Liu, Yantao Zhao
Formal analysis: Xinqiang Zhao
Investigation: Xinqiang Zhao
Methodology: Xinqiang Zhao
Project administration: Kun Ding
Resources: Yantao Zhao, Zhenggang Bi
Software: Xinqiang Zhao
Supervision: Yantao Zhao, Zhenggang Bi
Validation: Xinqiang Zhao
Visualization: Zhen Huang
Writing–original draft: Xinqiang Zhao
Writing–review & editing: Xiaoning Liu, Yantao Zhao, Zhenggang Bi
All authors have read and approved the final manuscript.

Ethics approval and consent to participate

This study was approved by the Animal Care and Use Committee of Beijing Vital River Laboratory Animal Technology Co., Ltd. (Approval No. AWE2022060305).

Consent for publication

Not applicable.

Availability of data

The datasets generated and/or analyzed during the current study are available from the corresponding author on reasonable request.

References

1. Qiao Z, Lian M, Han Y, et al. Bioinspired stratified electrowritten fiber-reinforced hydrogel constructs with layer-specific induction capacity for functional osteochondral regeneration. *Biomaterials.* 2021;266:120385.
2. Richter DL, Tanksley JA, Miller MD. Osteochondral autograft transplantation: a review of the surgical technique and outcomes. *Sports Med Arthrosc Rev.* 2016;24(2):74-78.
3. Lin X, Zhang Y, Li J, et al. Biomimetic multizonal scaffolds for the reconstruction of zonal articular cartilage in chondral and osteochondral defects. *Bioact Mater.* 2025;43:510-549. doi: 10.1016/j.bioactmat.2024.10.001
4. Sherman SL, Thyssen E, Nuelle CW. Osteochondral autologous transplantation. *Clin Sports Med.* 2017;36(3):489-500.
5. Wang Z, Li Z, Li Z, et al. Cartilaginous extracellular matrix derived from decellularized chondrocyte sheets for the reconstruction of osteochondral defects in rabbits. *Acta Biomater.* 2018;81:129-145.
6. Farr J, Gracitelli GC, Shah N, et al. High failure rate of a decellularized osteochondral allograft for the treatment of cartilage lesions. *Am J Sports Med.* 2016;44(8):2015-2022. doi: 10.1177/0363546516645086
7. Ladegaard Skov A. Like cartilage, but simpler. *Nature.* 2015;517(7532):25-26.
8. Hu X, Xu J, Li W, et al. Therapeutic “tool” in reconstruction and regeneration of tissue engineering for osteochondral repair. *Appl Biochem Biotechnol.* 2020;191(2):785-809. doi: 10.1007/s12010-019-03214-8

9. Zhang B, Huang J, Narayan RJ. Gradient scaffolds for osteochondral tissue engineering and regeneration. *J Mater Chem B.* 2020;8(36):8149-8170.

10. Mendes LF, Katagiri H, Tam WL, et al. Advancing osteochondral tissue engineering: bone morphogenetic protein, transforming growth factor, and fibroblast growth factor signaling drive ordered differentiation of periosteal cells resulting in stable cartilage and bone formation in vivo. *Stem Cell Res Ther.* 2018;9(1):42.
doi: 10.1186/s13287-018-0787-3

11. Sacks D, Baxter B, Campbell BC, et al. Multisociety consensus quality improvement revised consensus statement for endovascular therapy of acute ischemic stroke. *Int J Stroke.* 2018;13(6):612-632.

12. Aravamudhan A, Ramos DM, Nip J, et al. Osteoinductive small molecules: growth factor alternatives for bone tissue engineering. *Curr Pharm Des.* 2013;19(19):3420-3428.
doi: 10.2174/1381612811319190008

13. Xiao H, Huang W, Xiong K, et al. Osteochondral repair using scaffolds with gradient pore sizes constructed with silk fibroin, chitosan, and nano-hydroxyapatite. *Int J Nanomedicine.* 2019;14:2011-2027.
doi: 10.2147/IJN.S191627

14. Yin L, Wu Y, Yang Z, et al. Characterization and application of size-sorted zonal chondrocytes for articular cartilage regeneration. *Biomaterials.* 2018;165:66-78.

15. Bauza-Mayol G, Quintela M, Brozovich A, et al. Biomimetic scaffolds modulate the posttraumatic inflammatory response in articular cartilage contributing to enhanced neoformation of cartilaginous tissue in vivo. *Adv Healthc Mater.* 2022;11(1):2101127.
doi: 10.1002/adhm.202101127

16. Liang C, Wang G, Liang C, et al. Hierarchically patterned triple-layered gelatin-based electrospun membrane functionalized by cell-specific extracellular matrix for periodontal regeneration. *Dent Mater.* 2024;40(1):90-101.
doi: 10.1016/j.dental.2023.10.022

17. Wang P, Zhao Z, Li Z, et al. Attenuation of osteoarthritis progression via locoregional delivery of Klotho-expressing plasmid DNA and tanshinone IIA through a stem cell-homing hydrogel. *J Nanobiotechnol.* 2024;22(1):325.
doi: 10.1186/s12951-024-02608-z

18. Zhang G, He S, He X, et al. Local recruitment of autologous stem cells via a targeting microgel for precise cartilage repair without surgery. *Adv Mater.* 2025;37(33):2505544.
doi: 10.1002/adma.202505544
19. Gao F, Xu Z, Liang Q, et al. Osteochondral regeneration with 3D-printed biodegradable high-strength supramolecular polymer reinforced-gelatin hydrogel scaffolds. *Adv Sci (Weinh).* 2019;6(15):1900867.
doi: 10.1002/advs.201900867
20. Deng C, Zhu H, Li J, et al. Bioactive scaffolds for regeneration of cartilage and subchondral bone interface. *Theranostics.* 2018;8(7):1940.
21. Castilho M, Mouser V, Chen M, et al. Bi-layered micro-fibre reinforced hydrogels for articular cartilage regeneration. *Acta Biomater.* 2019;95:297-306.
22. Chen L, Deng C, Li J, et al. 3D printing of a lithium-calcium-silicate crystal bioscaffold with dual bioactivities for osteochondral interface reconstruction. *Biomaterials.* 2019;196:138-150.
23. Wang K, Liu L, Xie J, et al. Facile strategy to generate aligned polymer nanofibers: effects on cell adhesion. *ACS Appl Mater Interfaces.* 2018;10(2):1566-1574.
doi: 10.1021/acsami.7b16057
24. Li S, Sun B, Li X, Yuan X. Characterization of electrospun core/shell poly(vinyl pyrrolidone)/poly(L-lactide-co-ε-caprolactone) fibrous membranes and their cytocompatibility in vitro. *J Biomater Sci Polym Ed.* 2008;19(2):245-258.
doi: 10.1163/156856208783432499
25. Xu Y, Li D, Yin Z, et al. Tissue-engineered trachea regeneration using decellularized trachea matrix treated with laser micropore technique. *Acta Biomater.* 2017;58:113-121.
26. Fu L, Li P, Li H, et al. The application of bioreactors for cartilage tissue engineering: advances, limitations, and future perspectives. *Stem Cells Int.* 2021;2021(1):6621806.
doi: 10.1155/2021/6621806
27. Yang Z, Li H, Tian Y, et al. Biofunctionalized structure and ingredient mimicking scaffolds achieving recruitment and chondrogenesis for staged cartilage regeneration. *Front Cell Dev Biol.* 2021;9:655440.
28. Wang X, Song X, Li T, et al. Aptamer-functionalized bioscaffold enhances cartilage repair by improving stem cell recruitment in osteochondral defects of rabbit knees. *Am J Sports Med.* 2019;47(10):2316-2326.

doi: 10.1177/0363546519856355

29. Huang H, Zhang X, Hu X, et al. A functional biphasic biomaterial homing mesenchymal stem cells for in vivo cartilage regeneration. *Biomaterials.* 2014;35(36):9608-9619.

30. Zhu M, Jin J, Seddiqi H, et al. Novel three-dimensional preclinical model for investigating cartilage regeneration, incorporating physiological and pathological mechanical loading. *Tissue Eng Part C Methods.* 2025;31(10):367-379.
doi: 10.1177/19373384251390654

31. Chen M, Feng Z, Guo W, et al. PCL-MECM-based hydrogel hybrid scaffolds and meniscal fibrochondrocytes promote whole meniscus regeneration in a rabbit meniscectomy model. *ACS Appl Mater Interfaces.* 2019;11(44):41626-41639.
doi: 10.1021/acsami.9b13611

32. Vikingsson L, Claessens B, Gómez-Tejedor JA, et al. Relationship between micro-porosity, water permeability and mechanical behavior in scaffolds for cartilage engineering. *J Mech Behav Biomed Mater.* 2015;48:60-69.
doi: 10.1016/j.jmbbm.2015.03.021

33. Shen C, Zhou Z, Li R, et al. Silk fibroin-based hydrogels for cartilage organoids in osteoarthritis treatment. *Theranostics.* 2025;15(2):560.

34. Li S, Sun H, Lu Q, et al. Bionic ECM scaffolds for directional articular hyaline cartilage regeneration and long-term homeostasis maintenance. *Biomater Adv.* 2025;173:214292.

35. Mirmusavi MH, Ahmadian M, Karbasi S. Polycaprolactone-chitosan/multi-walled carbon nanotube: a highly strengthened electrospun nanocomposite scaffold for cartilage tissue engineering. *Int J Biol Macromol.* 2022;209:1801-1814.
doi: 10.1016/j.ijbiomac.2022.04.152

36. Ghadirian S, Shariati L, Karbasi S. Evaluation of the effects of cartilage decellularized ECM in optimizing PHB-chitosan-HNT/chitosan-ECM core-shell electrospun scaffold: physicochemical and biological properties. *Biomater Adv.* 2025;172:214249.
doi: 10.1016/j.bioadv.2025.214249

37. Wei W, Ma Y, Yao X, et al. Advanced hydrogels for the repair of cartilage defects and regeneration. *Bioact Mater.* 2021;6(4):998-1011.
doi: 10.1016/j.bioactmat.2020.09.030

38. Nordberg RC, Bielajew BJ, Takahashi T, et al. Recent advancements in cartilage tissue engineering innovation and translation. *Nat Rev Rheumatol.* 2024;20(6):323-346.

Appendix

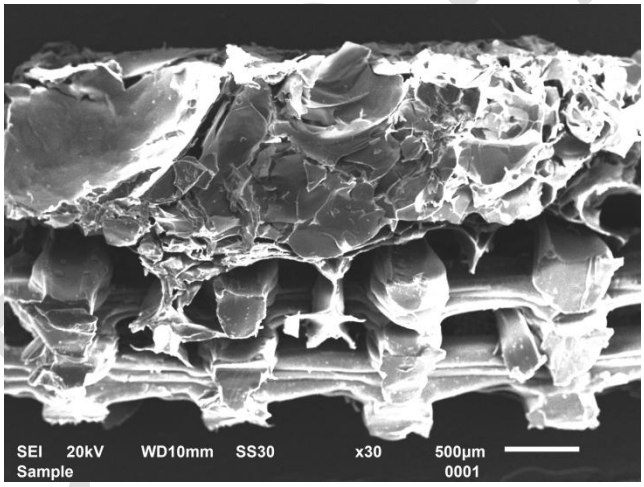

Figure A1. Representative SEM image showing the interface structure of the E/E7-PCL scaffold.